2-Arachidonoylglycerol mobilization following brief synaptic stimulation in the dorsal lateral striatum requires glutamatergic and cholinergic neurotransmission

Daniel J. Liput [a,b], Henry L. Puhl [a], Ao Dong [c,d,e], Kaikai He [c,d], Yulong Li [c,d,e,f], David M. Lovinger [b,*]

[a] *Laboratory of Molecular Physiology and National Institute on Alcohol Abuse and Alcoholism, National Institutes of Health, Maryland, 20852, USA*
[b] *Laboratory for Integrative Neuroscience, National Institute on Alcohol Abuse and Alcoholism, National Institutes of Health, Maryland, 20852, USA*
[c] *State Key Laboratory of Membrane Biology, Peking University School of Life Sciences, Beijing, 100871, China*
[d] *PKU-IDG/McGovern Institute for Brain Research, Beijing, 100871, China*
[e] *Peking-Tsinghua Center for Life Sciences, Beijing, 100871, China*
[f] *Chinese Institute for Brain Research, Beijing, 100871, China*

ARTICLE INFO

ABSTRACT

Several forms of endocannabinoid (eCB) signaling have been described in the dorsal lateral striatum (DLS), however most experimental protocols used to generate eCBs do not recapitulate the firing patterns of striatal-projecting pyramidal neurons in the cortex or firing patterns of striatal medium spiny neurons. Therefore, it is unclear if current models of eCB signaling in the DLS provide a reliable description of mechanisms engaged under physiological conditions. To address this uncertainty, we investigated mechanisms of eCB mobilization following brief synaptic stimulation that mimics *in vivo* patterns of neural activity in the DLS. To monitor eCB mobilization, the novel genetically encoded fluorescent eCB biosensor, GRAB$_{eCB2.0}$, was expressed presynaptically in corticostriatal afferents of C57BL6J mice and evoked eCB transients were measured in the DLS using a brain slice photometry technique. We found that brief bouts of synaptic stimulation induce long lasting eCB transients that were generated predominantly by 2-arachidonoylglycerol (2-AG) mobilization. Efficient 2-AG mobilization required coactivation of AMPA and NMDA ionotropic glutamate receptors and muscarinic M1 receptors. Dopamine D2 receptors expressed on cholinergic interneurons inhibited 2-AG mobilization by inhibiting acetylcholine release. Collectively, these data uncover unrecognized mechanisms underlying 2-AG mobilization in the DLS.

1. Introduction

The endocannabinoids (eCBs) are lipid-derived signaling molecules that play a major role in synaptic modulation in the central nervous system (CNS). Unlike traditional neurotransmitters that are released from presynaptic vesicles, the eCBs are produced via enzymatic catalysis of precursor phospholipids in the plasma membrane (Ueda et al., 2013). In the most common scenario, lipid metabolism occurs in the postsynaptic membrane and the eCBs traverse the synaptic cleft to stimulate CB1 receptors (CB1R) on presynaptic terminals, leading to inhibition of neurotransmitter release (Kano, 2014; Kreitzer and Regehr, 2001; Lovinger, 2008; Ohno-Shosaku et al., 2001; Wilson and Nicoll, 2001). The predominant mobilization mechanism for the two main eCBs,

2-arachidonoylglycerol (2-AG) and arachidonoylethanolamine (Anandamide, AEA), is production and release in response to membrane depolarization and subsequent Ca^{2+} influx, and/or activation of $G\alpha_{q/11}$ by g-protein coupled receptors (GPCRs).

The kinetics of eCB signaling have not been measured directly on time scales supporting synaptic modulation, but estimates have been proposed based on the onset and decay of eCB-dependent short term depression (STD) (Heinbockel et al., 2005). This measure involves not only the kinetics of extracellular eCB increases, but also the timing of receptor activation and presynaptic effector changes. Furthermore, although these estimates may be accurate for depolarization-induced suppression of inhibition (DSI) and other types of STD, the timing and magnitude of eCB signaling may not be universal for all forms of

---

eCB-dependent plasticity and may not be the same for 2-AG and AEA. Additionally, the kinetics of eCB signaling and the physiological consequences do not always correlate. For example, long term depression (LTD) at corticostriatal and hippocampal synapses lasts for more than an hour but becomes resistant to CB1R antagonists minutes after induction (Chevaleyre and Castillo, 2003; Ronesi et al., 2004; Yin et al., 2006). Therefore, strategies other than measuring plasticity kinetics are required to accurately measure eCB mobilization underlying physiological phenomena of interest.

CB1Rs and the appropriate eCB synthesis and degradation enzymes are abundantly expressed in the dorsal lateral striatum (DLS), and indeed multiple forms of eCB-dependent depression have been described in this brain region (Calabresi et al., 2007; Mathur and Lovinger, 2012). Perhaps the most well characterized form, LTD at corticostriatal synapses, can be induced by high frequency stimulation (HFS, Calabresi et al., 1992; Gerdeman et al., 2002) or low frequency stimulation (LFS, Ronesi and Lovinger, 2005). Interestingly, these two stimulation protocols may induce LTD by differentially mobilizing AEA or 2-AG, suggesting that different modes of eCB signaling can be engaged depending on the amount of neural activity (Lerner and Kreitzer, 2012). Although HFS or long bouts of LFS result in eCB-LTD in the DLS, these stimulation patterns do not accurately recapitulate the *in vivo* firing patterns of striatal-projecting pyramidal neurons in the cortex or firing patterns of medium spiny neurons (MSNs) in the striatum (Costa et al., 2004). In other brain regions, eCB-dependent plasticity can be induced by brief bouts of synaptic stimulation (Brown et al., 2003; Galante and Diana, 2004; Maejima et al., 2001, 2005), and eCBs should also be mobilized by physiologic patterns of afferent stimulation in the DLS. Indeed, brief cortical stimulation paired with post-synaptic depolarization induces a form of striatal long-term potentiation (LTP) that is dependent on eCB mobilization (Cui et al., 2015, 2016).

Optical techniques are rapidly emerging for the study of neuromodulation in *ex vivo* and *in vivo* models. In particular, intensity-based genetically encoded biosensors, based on the GPCR scaffold, are being implemented to uncover unrecognized physiological mechanisms across neurotransmitter systems (Liang et al., 2015; Mizuno et al., 2019; Ravotto et al., 2020; Wang et al., 2018). These new generation sensors have several desirable characteristics including inherent ligand specificity and affinity, rapid reporting dynamics, high spatial resolution, cellular targeting capability, and disabled effector coupling. A novel biosensor engineered on the GPCR platform, called GRAB$_{eCB2.0}$, was recently developed for detection of 2-AG and AEA (Dong et al., 2021). We used this sensor in an *ex vivo* brain slice photometry technique to study eCB mobilization kinetics, neural activity rules supporting eCB generation, and neurochemical pathways underlying eCB synthesis and degradation in the striatum.

2. Materials and methods

2.1. Animals

All animal studies were conducted in accordance with the National Institutes of Health's *Guidelines for Animal Care and Use* and all experimental protocols were approved by the National Institute on Alcohol Abuse and Alcoholism Animal Care and Use Committee. Male and female mice were used in this study. C57BL/6J and ChAT-IRES-Cre (B6.129S-Chat$^{tm1(cre)Lowl}$/MwarJ, Stock No: 031661) mice (8–10 weeks) were ordered from The Jackson Laboratory (Bar Harbor, ME, USA). Drd2$^{LoxP/LoxP}$(Drd2^{tm1Mrub}, Bello et al., 2011) mice (Bello et al., 2011) were maintained in house on a C57BL/6J background. To generate mice lacking D2Rs in cholinergic interneurons, mice heterozygous for the ChAT-IRES-Cre allele and homozygous for the Drd2LoxP allele (Drd2$^{LoxP/LoxP}$ChAT$^{IRES-Cre/WT}$) were bred with mice homozygous for the Drd2LoxP allele (Drd2$^{LoxP/LoxP}$). RGS9cre (Dang et al., 2006) and DAGLαflox (Shonesy et al., 2018) mice were maintained in house on a C57BL/6J background. To generate mice lacking DAGLα in MSNs, male

mice heterozygous for the RGS9cre allele and homozygous for the DAGLαflox allele were bred with female mice homozygous for the DAGLαflox allele. The RGS9cre allele was maintained only on male mice to avoid high rates of germline recombination observed when the allele is inherited from female mice (Liput, 2018). Genotypes were determined by polymerase chain reaction (PCR) using genomic DNA from ear biopsies.

2.2. Viral vectors

AAV2/9.hSyn.GRAB$_{eCB2.0}$.WPRE.hGHpolyA (Titer: 1.0×10^{13} GC/mL) and AAV2/9.hSyn.GRAB$_{eCBMUT}$.WPRE.hGHpolyA (Titer: 1.0×10^{13} GC/mL) were purchased from Vigene Biosciences (Rockville, MD, USA). AAV2/9.hSyn.GRAB$_{ACh3.0}$.WPRE.hGHpolyA (Titer: 2.4×10^{13} GC/mL) was packaged in house as described below. All viruses were aliquoted and stored at −80 °C.

2.3. Viral production

AAV vectors were produced using a helper free triple transfection procedure similar to that previously described (Xiao et al., 1998). 293AAV cells (Cell Biolabs, Inc) were cultured in Dulbecco's modified Eagle's medium (DMEM) with GlutaMAX (ThermoFisher, Waltham, MA, USA) and supplemented with non-essential amino acids (NEAA, Gibco™), 10% FBS (Gibco™) and antibiotics (100 μg/mL penicillin and μg/mL streptomycin, Gibco™). Cells were seeded at a density of ~80% in T175 tissue culture flasks and transfected with 0.165 μg pDNA/cm^2 in a 1:1:1 M ratio of pAAV2.hSyn.GRAB$_{ACh3.0}$.WPRE.hGHpolyA shuttle vector, pR/C9 and pHelper vectors (Cell Biolabs, San Diego, CA) complexed to polyethylenimine (PEI) (N/P ratio = 5). After 72 h cells were harvested, resuspended in FBS-free DMEM and lysed by repeated freeze/thaw cycles. The lysate was centrifuged at 10,000g for 20 min and the cleared supernatant was collected and incubated with benzonase (50U/mL, Sigma-Aldrich, St Louis, MO, USA) for 1 h at 37 °C. The cleared supernatant was then subject to ultracentrifugation through an iodixanol density gradient similar to previously described techniques (Strobel et al., 2015). Iodixanol gradients were layered in 13.2 mL thin wall tubes (14 × 89 mm, Beckman Coulter, Indianapolis, IN, USA). The iodixanol steps were layered in the following order: 1 mL 60% iodixanol, 1.8 mL 40% iodixanol, 2.2 mL 25% iodixanol, 3 mL 15% iodixanol w/1M NaCl. The cleared supernatant containing the AAV particles was layered on top of the gradient and centrifuged in a SW41 rotor (Beckman Coulter) at 41,000 RPM for 4.5 h at 10 °C. After ultracentrifugation, the 40% iodixanol layer containing purified AAV particles was collected and the iodixanol was exchanged for dPBS and concentrated to 100 μL. The AAV sample was passed through a 0.22 μm filter and analyzed by silver stain and quantitative PCR (qPCR).

An aliquot of purified virus was serial diluted, denatured in 1 M DDT and 1x lane marker for 5 min at 90 °C, and electrophoresed on a polyacrylamide gel. Gels were stained using a Pierce™ silver stain kit according to the manufacturer's instructions (ThermoFisher) and imaged using a FluorChem E system (ProteinSimple, San Jose, CA, USA). The presence of AAV particles was confirmed by visualization of the VP1, VP2 and VP3 capsid proteins and purity by the lack of other contaminating bands.

AAV titer, defined as genome copies (GC)/mL was determined by qPCR. 1 μL of AAV sample was diluted into 16 μL H$_2$0, 1 μL DNase I and 2 μL 10x DNase buffer (New England Biolabs, Ipswich, MA, USA), and incubated for 30 min at 37 °C. The DNase I treated sample was serial diluted (1:5, 1:20, 1:100, 1:500 and 1:2500) and stored on ice for qPCR. A standard curve, using a pAAV shuttle vector containing AAV2 ITRs, ranging from 2×10^5 to 2×10^9 plasmid copies was constructed for calculating the AAV titer. Three 5 μL replicates of each sample dilution and standard curve concentration were added to 15 μL of SYBR™ Green PCR master mix (ThermoFisher) containing 0.67 μM FWD and REV primers targeting the AAV2 ITRs. qPCR was performed on a

StepOnePlus™ system (ThermoFisher) using the following protocol: 3 min at 98 °C, (melt at 98 °C for 15 s, anneal/extend at 60 °C for 30 s) x 39 cycles. Melt curves were performed to verify a single amplification product. The C_T value was defined as the cycle number at which the amplification curve reached a ΔRn (Rn − baseline, where Rn is the fluorescence of the reporter dye divided by the fluorescence of a passive reference dye) threshold set at 0.1. A standard curve from the AAV2 plasmid standards (concentration by C_T) was plotted, fit with a line and the concentration of each AAV sample dilution was determined.

2.4. Surgery

Mice were anesthetized with isoflurane and stereotaxically injected with AAV vectors into motor cortex (100 nL, coordinates relative to bregma in mm: A/P: + 1.1; M/L: ± 1.7; D/V: 1.6) or DLS (300 nL, coordinates relative to bregma in mm: A/P: + 0.75; M/L: ± 2.5; D/V: 3.5) at a rate of 25–50 nL/min, using a 7000 series 0.5 μL Hamilton syringe (Hamilton Company, Reno, NV, USA) and Pump 11 Elite Nanomite (Harvard Apparatus, Holliston, MA, USA) syringe pump. Following surgery, mice were given an injection of Ketoprofen (5 mg/kg, s.c.) and postoperative care was provided for at least two days and until mice regained their preoperative weight.

2.5. Slice photometry

Mice, 4–6 weeks after viral infusion, were deeply anesthetized with isoflurane, decapitated and the brains extracted and placed in ice cold sucrose cutting solution (in mM): 194 sucrose, 30 NaCl, 4.5 KCl, 26 NaHCO$_3$, 1.2 NaH$_2$PO$_4$, 10 D-glucose, 1 MgCl$_2$ saturated with 5% CO$_2$/ 95% O$_2$. Coronal brain slices (250 μm) were prepared with a Leica VT1200S Vibratome (Leica Microsystems, Buffalo Grove, IL) and slices were incubated at 32 °C for 40–60 min in aCSF (in mM): 124 NaCl, 4.5 KCl, 26 NaHCO$_3$, 1.2 NaH$_2$PO$_4$, 10 D-glucose, 1 MgCl$_2$, 2 CaCl$_2$. After incubation at 32 °C, slices were held at room temperature until transfer to a recording chamber.

Photometry recordings were acquired using a Zeiss Axioscope or Olympus BX41 upright epifluorescence microscope equipped with a 40 × 0.8 NA water emersion objective. Slices were placed in a recording chamber and superfused at ~2 mL min^{-1} with aCSF warmed to 29–31 °C. This temperature was chosen based on preliminary experiments to improve the stability of evoked eCB transients over the course of a 60–90 min pharmacological experiment. A twisted bipolar polyimide-coated stainless-steel stimulating electrode (~200 μm tip separation) was placed in the DLS just medial to the corpus callosum and slightly below the tissue surface in a region with visible fluorescence. Placing the stimulating electrode in the DLS, rather than the corpus callosum or sensorimotor cortex, resulted in reliable evoked eCB transients. Importantly, this placement is not expected to influence eCB mobilization mechanisms as optogenetic stimulation of extrinsic glutamate afferents leads to release of acetylcholine, dopamine and glutamate (Kosillo et al., 2016; Mateo et al., 2017), similar to local electical stimulation.

Using the 40× objective, focus was adjusted to just below the tissue surface, at a similar height as the electrode tips. GRAB sensors were excited using either a mercury HBO 100 lamp equipped with a Zeiss FluoArc variable intensity lamp controller (Carl Zeiss Microcopy GmbH, Jena, Germany) and gated with a uniblitz shutter (Vincent Associates, Rochester, NY, USA), or a 470 nm light emitting diode (LED, ThorLabs, Newton, NJ, USA). The Zeiss axiovert system was equipped with a Zeiss 38 HE filter set (Ex. 470/40, FT 495, Em. 525/50), and the Olympus BX41 was equipped with a FITC filter set (Ex. 475/28, FT 495, Em. 520/ 35). Excitation power was measured at the sample plane using a microscope slide photodiode power sensor (ThorLabs) and was 3.8 mW for the mercury HBO lamp and <1.0 mW for the 470 nm LED. A 180 μm^2 aperture located in the light path between the microscope and photomultiplier tube (PMT) was used so photons were collected from a region

of interest just medial to the stimulation electrode tips. Photons passing through the aperture were directed to a PMT (Model D-104, Photon Technology International, Edison, NJ, USA) with the cathode voltage set to 300–400 V. The PMT output was amplified (gain: 0.1 μA/V; time constant: 5 msec), filtered at 50 Hz and digitized at 250 Hz using a Digidata 1322A or a 1550B and Clampex software (Axon Instruments, Molecular Devices LLC, Sunnyvale, CA, USA). For all experiments, electrical stimulation and GRAB sensor measurements were acquired as discrete trials repeated every 3 min. For each trial, the light exposure period was 35–45 s to minimize sensor photobleaching, while capturing peak responses and most of the decay phase (Fig. 1D). To evoke an eCB or ACh transient, a burst of electrical pulses (1.0–1.5 mA, 200–500 μs) was delivered 5 s after initiating fluorophore excitation. Transients were calculated as $\Delta F/F$ by averaging the PMT voltage (V) for a period of 1 s just prior to electrical stimulation (F) and then calculating V/F-1 for each digitized data sample.

2.6. Immunohistochemistry

Mice were anesthetized with isofluorane and transcardially perfused with 20 mL of 0.1 M phosphate buffered saline (PBS, pH 7.4) followed by 20 mL of 4% formaldehyde in PBS. Following perfusion, brains were extracted and post-fixed in 4% formaldehyde overnight at 4 °C. Brains were serial sectioned (1:6) at 40 μm on the coronal plane and stored in cryoprotectant (30% glycerol and 30% ethylene glycol in 0.1 M phosphate buffer, pH = 7.4) at −20 °C until further processing. Sections were removed from cryoprotectant and rinsed 3 × 5 min in PBS. Next, sections were permeabilized and blocked for 1 h at RT using a blocking solution consisting of 5% bovine serum albumin (BSA) and 0.2% Triton-X 100 in PBS. Following blocking, sections were incubated in chicken anti-GFP primary antibodies (Abcam Cat# ab92456; 500 μg/mL IgY polyclonal diluted at 1:3000 in blocking solution) for approximately 24 h at 4 °C. After primary antibody incubation, sections were rinsed 3 × 10 min in PBS and transferred to Alexa Fluor®-488 donkey anti-Chicken (1:1000) secondary antibodies for 1 h at RT. Finally, sections were rinsed 4 × 10 min in PBS (first rinse contained DAPI stain). Following IHC, sections were mounted and coverslipped with No. 1.5 cover glass and Fluoromount G (RI = 1.40, Electron Microscopy Sciences). Low magnification epifluorescence images were acquired with a Zeiss Axiozoom microscope (Carl Zeiss, Oberkochen, German) equipped with a Zeiss Axiocam MR monochrome CCD camera. For confocal imaging, a Zeiss LSM 880 confocal microscope equipped with 405–30 diode and argon ion lasers for 405 nm and 488 nm excitation, respectively and a Zeiss Plan-Apochromat 63× oil immersion objective (1.4 NA) was used. Images were acquired with the pinhole adjusted to 1.0 AU. ImageJ software (v.1.48) was used to adjust contrast of images for presentation in figures.

2.7. Drugs

Drugs were dissolved in DMSO or dH$_2$O at stock concentrations, aliquoted and stored at −20 °C. Just prior to use, drugs were diluted to working concentrations in aCSF. The final concentration of DMSO was <0.02%, a concentration that did not affect evoked eCB transients. β-Cyclodextrin (3.0 mg/50 mL, MilliporeSigma, Burlington, MA, USA) was included as a carrier for AM251 and DO34 solutions. The compounds AM251, URB597, JZL184, (−)-Quinpirole hydrochloride, VU 0255035, (RS)-3,5-Dihyroxyphenylglycine (DHPG), 6,7-Dinitroquinoxaline-2,3-dione (DNQX) disodium salt, DL-2-Amino-5-phosphonopentanoic acid (DL-AP5), JNJ16259685 and 2-Methyl-6-(phenylethynyl)pyridine (MPEP) hydrochloride were purchased from Tocris (Minneapolis MN, USA). (±)-Sulpiride was purchased from MilliporeSigma. DO34 was purchased from Aobious (Gloucester, MA, USA). VU 0486846 was generously provided by Dr. Jeffery Conn (Vanderbilt University, Nashville, TN, USA).
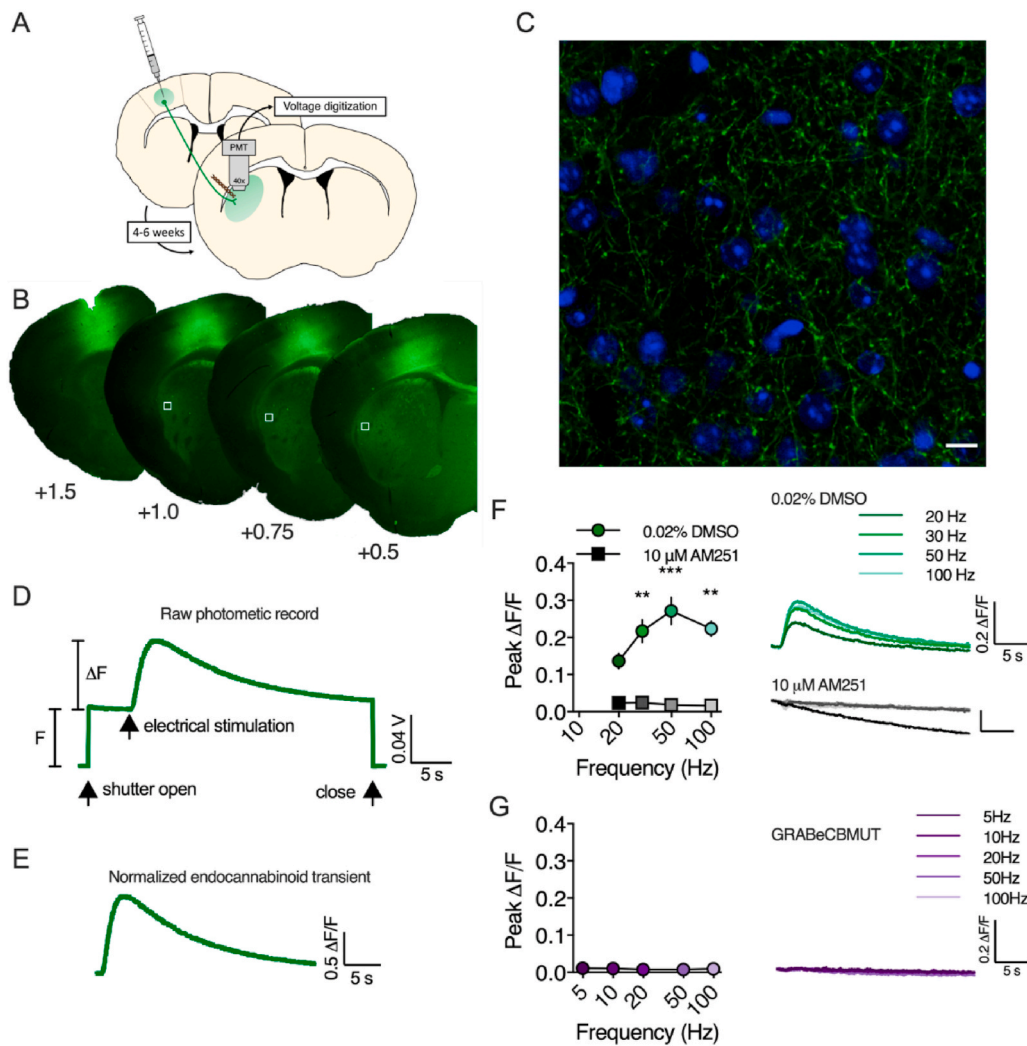
Fig. 1. GRAB$_{eCB2.0}$ detects eCB transients in brain slice. A) AAV vectors encoding GRAB$_{eCB2.0}$ were infused into motor cortex (M1/M2) and fluorescence from corticostriatal afferents was measured in the DLS. B) Representative fluorescent micrographs of GRAB$_{eCB2.0}$ expression at the injection site in M1/M2 and in corticostriatal afferents in the DLS. White boxes indicate approximate recording sites. C) Confocal micrograph of GRAB$_{eCB2.0}$ (green) expression in corticostriatal afferents in the DLS (blue, DAPI; scale bar = 10 μm). D) Raw photometric recording labeled to indicate F and ΔF measurements, epifluorescence exposure time (shutter open/close) and timing of electrical stimulation. E) Normalized eCB transient evoked by a train of electrical stimuli. F) GRAB$_{eCB2.0}$ fluorescent transients evoked by 1s train stimulation at varying frequencies in slices preincubated in either the CB1R antagonist, AM251, or DMSO vehicle. G) Results of 1 s train stimulation in slices expressing the GRAB$_{eCBMUT}$ control sensor that does not bind eCBs. **, p < 0.01, ***p < 0.001.

2.8. Data analysis

Slice photometry raw data were collected and analyzed using the pClamp™ software suit (v9.2 and v10; Molecular Devices, San Jose, CA, USA). Photometry sweeps were exported to Microsoft Excel (v16.3; Redmond, WA, USA) to calculate normalized ΔF/F traces, peak ΔF/F values, eCB mobilization time and % baseline timecourse data. Rise $t_{1/2}$ was calculated in Graphpad Prism (v8.3; San Diego, CA, USA) by fitting the rising phase of the eCB transient with an asymmetrical logistic curve. Statistical analysis and graph rendering were performed using Graphpad Prism. Baseline normalized timecourse data were analyzed using one sample t-tests, 1-way rmANOVAs followed by Tukey's multiple comparisons test, 2-way rmANOVAs followed by Sidak's multiple comparisons test or mixed-effects ANOVA followed by Sidak's multiple comparisons test. For t-tests and 1-way rmANOVA analysis, baseline was the average peak ΔF/F of 5 predrug sweeps (for 1-way ANOVA only), drug condition was the average peak ΔF/F of the last two data points of the drug application period (except for (RS)-DHPG experiments where only the sweep with the highest peak ΔF/F was used) and washout/antagonist wash (for 1-way ANOVA only) was the average of the last two data points during that period. For all experiments, n represents the number of brain slices. Data are plotted as mean ± standard error of the mean.

3. Results

The novel genetically encoded biosensor, GRAB$_{eCB2.0}$, detects eCB transients evoked by electrical stimulation in the DLS.

To study eCB mobilization in the DLS, we used an *ex vivo* brain slice photometry technique similar to published reports using GCaMP calcium sensors (Kupferschmidt and Lovinger, 2015; Sgobio et al., 2014). AAV2/9.hSyn.GRAB$_{eCB2.0}$ and AAV2/9.hSyn.GRABe$_{CBMUT}$ vectors were infused into motor cortex (M1/M2) of wildtype C57BL/6J mice and ~4–6 weeks later, eCB transients were measured at corticostriatal afferents in the DLS (Fig. 1A–E).

Fluorescent transients from GRAB$_{eCB2.0}$ were evoked by 1s train stimulation and the amplitude of these transients increased with higher stimulation frequencies up to 100 Hz (n = 3, Fig. 1F). To confirm the specificity of the fluorescent transients, slices were preincubated in AM251 (10 μM) for ~1 h before performing photometry experiments. In these slices, fluorescent transients were not detected in response to train stimulation up to 100Hz (n = 3 slices/group, 2-way RM ANOVA, Drug: $F_{(1,8)} = 113.8$, p < 0.0001; Frequency: $F_{(3,8)} = 5.9$, p < 0.020; Interaction: $F_{(3,8)} = 2.6$, p > 0.05). Additionally, evoked eCB transients could not be measured with the GRAB$_{eCBMUT}$ sensor (n = 6, Fig. 1G), which contains the mutation F177A that greatly reduces 2-AG and AEA affinity, demonstrating that the fluorescent transients measured with GRAB$_{eCB2.0}$ are dependent on agonist occupancy of the orthosteric binding site of CB1R contained within the sensor.

In the cerebellum, brief stimulation of parallel fibers (i.e. 5 or 10

pulses at 50 Hz) triggers eCB mobilization and short-term depression (Brown et al., 2003; Maejima et al., 2001). We tested whether similar stimulation protocols are sufficient to activate eCB production in the DLS. Indeed, eCB transients could be measured in response to brief trains of electrical stimulation (Fig. 2). Paired-pulse stimulation evoked small, but measurable, eCB transients that increased slightly in amplitude at higher frequencies. Trains of 5 or 10 pulses evoked larger transients that were augmented by increasing the stimulation frequency up to 100 Hz (Fig. 2A&B). The eCB transients developed over several seconds measured from the start of train stimulation, with a mean $t_{1/2}$ rise time of 1.4 ± 0.03 s regardless of stimulation frequency (Fig. 2C). The eCB decay phase was well described by a single exponential function and was similar across all stimulation pulse numbers and frequencies with a

mean tau of 13.7 ± 0.3 s (Fig. 2D).

There was a notable delay between the start of synaptic stimulation and any measurable increase in $GRAB_{eCB2.0}$ fluorescence, which we refer to as the eCB mobilization time or t_{eCB} (Fig. 2E and F). The t_{eCB} represents the cumulative time from the start of synaptic stimulation and recruitment of postsynaptic eCB production machinery, to retrograde eCB transit and binding to the $GRAB_{eCB2.0}$ sensor. Thus, this measurement may correlate with the minimum time required for eCB-dependent presynaptic inhibition (Heinbockel et al., 2005). The t_{eCB} was measured from the start of train stimulation to the time at which the presynaptic $GRAB_{eCB2.0}$ fluorescence reached a threshold set at 3x rms of the baseline fluorescence and was 0.301 ± 0.01 s regardless of stimulation frequency (Fig. 2F).
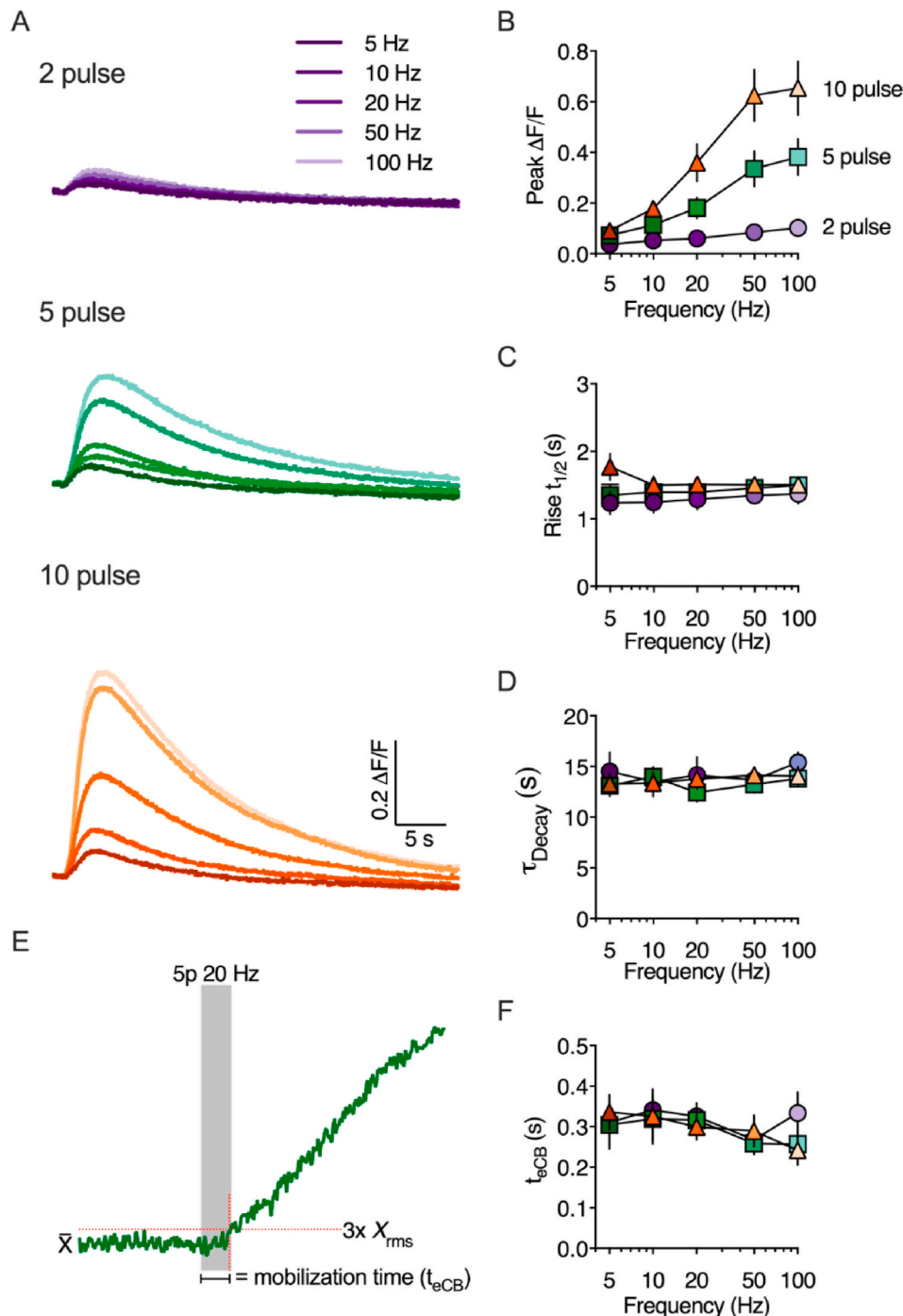

Fig. 2. Evoked eCB transients are modulated by stimulation pulse number and frequency. A) Representative traces of eCB transients evoked by brief trains of synaptic stimulation. B-D) Quantification of peak amplitude, rise time (defined as the time to reach 50% of the peak amplitude) and decay kinetics as a function of stimulation pulse number and frequency. E) Schematic illustrating the calculation of eCB mobilization time (t_{eCB}). Representative eCB transient evoked by a 5 pulse train at 20 Hz. F) Quantification of t_{eCB} as a function of stimulation pulse number and frequency.

3.1. 2-AG is the predominant eCB mobilized by brief synaptic stimulation in the DLS

Previous studies have shown that both 2-AG and AEA can be generated by synaptic stimulation in the striatum, but which eCB predominates depends on the specific experimental induction protocol used (Lerner and Kreitzer, 2012). To investigate whether 2-AG and/or AEA are mobilized by brief synaptic stimulation, we measured the effect of monoacylglycerol lipase (MAGL) or fatty acid amide hydrolase (FAAH) inhibition on eCB transients evoked by a 5-pulse burst at 20Hz (Fig. 3). Over the course of 75 min, JZL184 (2 μM, Fig. 3A–C), prolonged the eCB transient decay rate ($321 \pm 69.9\%$ of baseline, n = 5 slices, 1 sample t-test, $t_{(4)} = 3.164$, $p < 0.034$), consistent with inhibition of 2-AG degradation. Additionally, the basal fluorescence, F, tended to increase ($155.3 \pm 21.8\%$ of baseline, n = 6 slices, 1 sample t-test, $t_{(5)} = 2.535$, $p = 0.052$), indicating that MAGL inhibition generates a 2-AG tone in the DLS. In contrast, bath application of URB597 (1 μM, Fig. 3D–F) did not significantly prolong the decay rate of the evoked eCB transient ($134.6 \pm 14.8\%$ of baseline, n = 5 slices, $p > 0.05$), or change the basal fluorescence ($108.1 \pm 4.4\%$ of baseline, n = 5 slices, $p > 0.05$). To confirm that the eCB transients evoked by brief synaptic stimulation were primarily 2-AG, we tested whether diacylglycerol lipase (DAGL) inhibition would inhibit the transients evoked by 5 pulse bursts at 20 Hz (Fig. 3G and H). Indeed, preincubating slices in the DAGL inhibitor, DO34 (1 μM), for ~1 h significantly reduced the peak amplitude of the eCB transient over a range of stimulation intensities (n = 5/6 slices, 2-way RM-ANOVA, Drug: $F_{(1,9)} = 48.31$, $p < 0.0001$; Stimulation amplitude: $F_{(6,54)} = 76.11$, $p < 0.0001$; Interaction: $F_{(6,54)} = 34.23$, $p < 0.0001$). DO34 did not completely abolish evoked eCB transients, which could be due to incomplete inhibition of DAGL or indicate some AEA production. Additionally, the source of 2-AG production cannot be determined with pharmacological inhibition of DAGL. To address these questions, we bred DAGLαflox mice with RGS9cre mice to conditionally knockout DAGLα from striatal MSNs (MSN-DAGLαKO). In slices from MSN-DAGLαKO mice, 2-AG transients could not be evoked over a range of stimulation intensities, while 2-AG transients were evoked in slices from DAGLαWT mice in a intensity dependent fashion, similar to observations with slices from C57BL6J wildtype mice (Fig. 3I–J, n = 5/6 slices, mixed-effects ANOVA, Genotype: $F_{(1,8)} = 13.8$, $p < 0.01$;

Stimulation amplitude: $F_{(7,54)} = 22.28$, $p < 0.0001$; Interaction: $F_{(7,54)} = 19.95$, $p < 0.0001$).

3.2. Metabotropic and ionotropic glutamate receptors contribute to 2-AG mobilization following brief synaptic stimulation

Group I mGluRs induce eCB-dependent plasticity at many synapses in the brain, including the corticostriatal synapse (Calabresi et al., 1992; Gubellini et al., 2001; Kreitzer and Malenka, 2005; Sung et al., 2001). In the DLS, mGlu1 and mGlu5 are implicated in HFS-LTD and exogenous activation mGlu1/5 induces eCB-LTD (Kreitzer and Malenka, 2005). Therefore, we tested whether 2-AG production evoked by brief synaptic stimulation (5p 20Hz) involved recruitment of mGlu1 and/or mGlu5 (Fig. 4). Bath application of the mGlu1 negative allosteric modulator (NAM), JNJ16259685 (JNJ'685, 1 μM), reduced the amplitude of the 2-AG transient to $83.9 \pm 6.1\%$ of baseline (Fig. 4A–C, n = 5 slices, 1-way RM ANOVA, Drug: $F_{(2,8)} = 5.531$, $p < 0.031$) and bath application of the mGlu5 NAM, MPEP (10 μM), reduced the amplitude of the 2-AG transient to $79.8 \pm 6.0\%$ of baseline (Fig. 4D–F, n = 5 slices, 1-way RM ANOVA, Drug: $F_{(2,8)} = 12.14$, $p < 0.004$). Given the role of mGlu1 and mGlu5 in evoked 2-AG transients, we tested whether activation of mGlu1/5 with an exogenous agonist could enhance the 2-AG transient. Bath application of (RS)-DHPG (100 μM) caused a biphasic change in the amplitude of the evoked 2-AG transient (Fig. 4G–I, n = 5 slices, 1-way RM ANOVA, Drug: $F_{(2,8)} = 97.33$, $p < 0.0001$). The maximum augmentation was $173.3 \pm 7.4\%$ of baseline, which occurred during the first evoked transient following (RS)-DHPG application (n = 5, $p < 0.0001$). This modulation subsequently decayed over time with the 2-AG amplitude plateauing at $75.3 \pm 4.1\%$ of baseline (n = 5, $p < 0.023$). The baseline fluorescence intensity (F, as defined in Fig. 1c) was not changed by (RS)-DHPG (data not shown). Collectively, these results show that group I mGluRs can couple to 2-AG generation mechanisms as previously demonstrated in the DLS using electrophysiology approaches, and that mGlu1 and mGlu5 activation contributes to 2-AG generation following brief synaptic stimulation.

Postsynaptic depolarization and activation of voltage gated calcium channels is required for many forms of eCB dependent STD and LTD. One presumed source of depolarization for synaptically-driven eCB generation is ionotropic AMPA receptors (AMPARs) (Brown et al.,
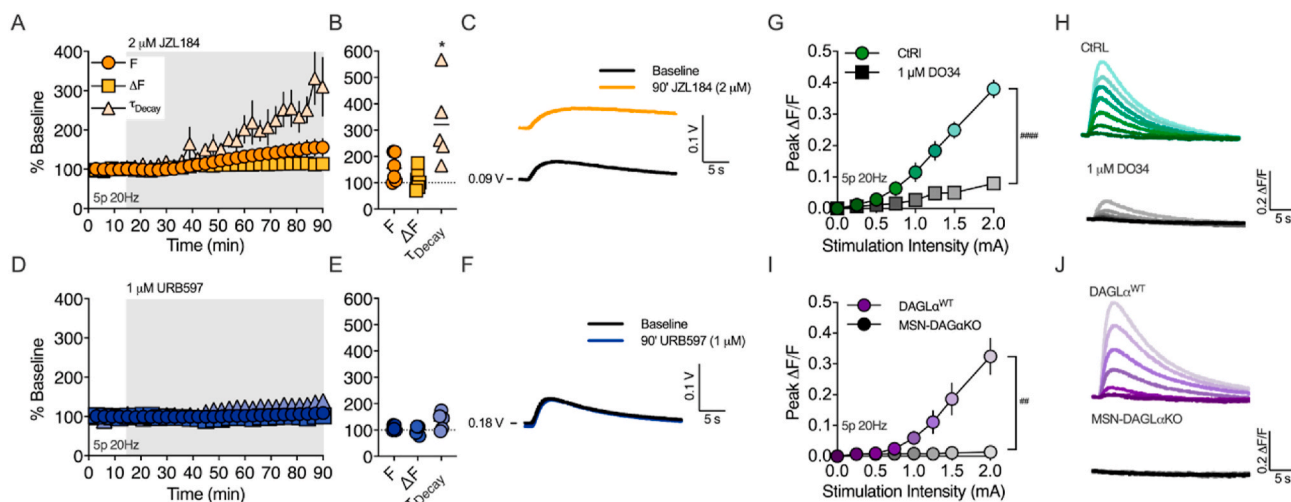

Fig. 3. 2-AG is the main eCB mobilized by brief synaptic stimulation. A) Timecourse of MAGL inhibitor, JZL184, on basal fluorescence (F), evoked peak ΔF and transient decay (τ_{decay}). B) Effect of JZL184 after 75 min of bath application. C) Representative traces of unnormalized GRABeCB2.0 fluorescence before and after JZL184 with baseline PMT voltage (V) indicated. D) Same as in panel A but with the FAAH inhibitor, URB597. E) Effect of URB597 after 75 min of bath application. F) Representative traces of unnormalized GRABeCB2.0 fluorescence before and after URB597. G) Peak amplitude of eCB transients evoked in slices preincubated in the DAGL inhibitor, DO34, or VEH. eCB transients were evoked using a 5 pulse train at 20Hz at indicated stimulation intensities. H) Representative eCB transients at increasing stimulation intensities. I) Peak amplitude of eCB transients evoked in slices from DAGLα^WT control mice or slices from MSN-DAGLαKO mice. J) Representative eCB transients at increasing stimulation intensities. *, $p < 0.05$ compared to baseline, ##, <0.01 and ###, <0.001.
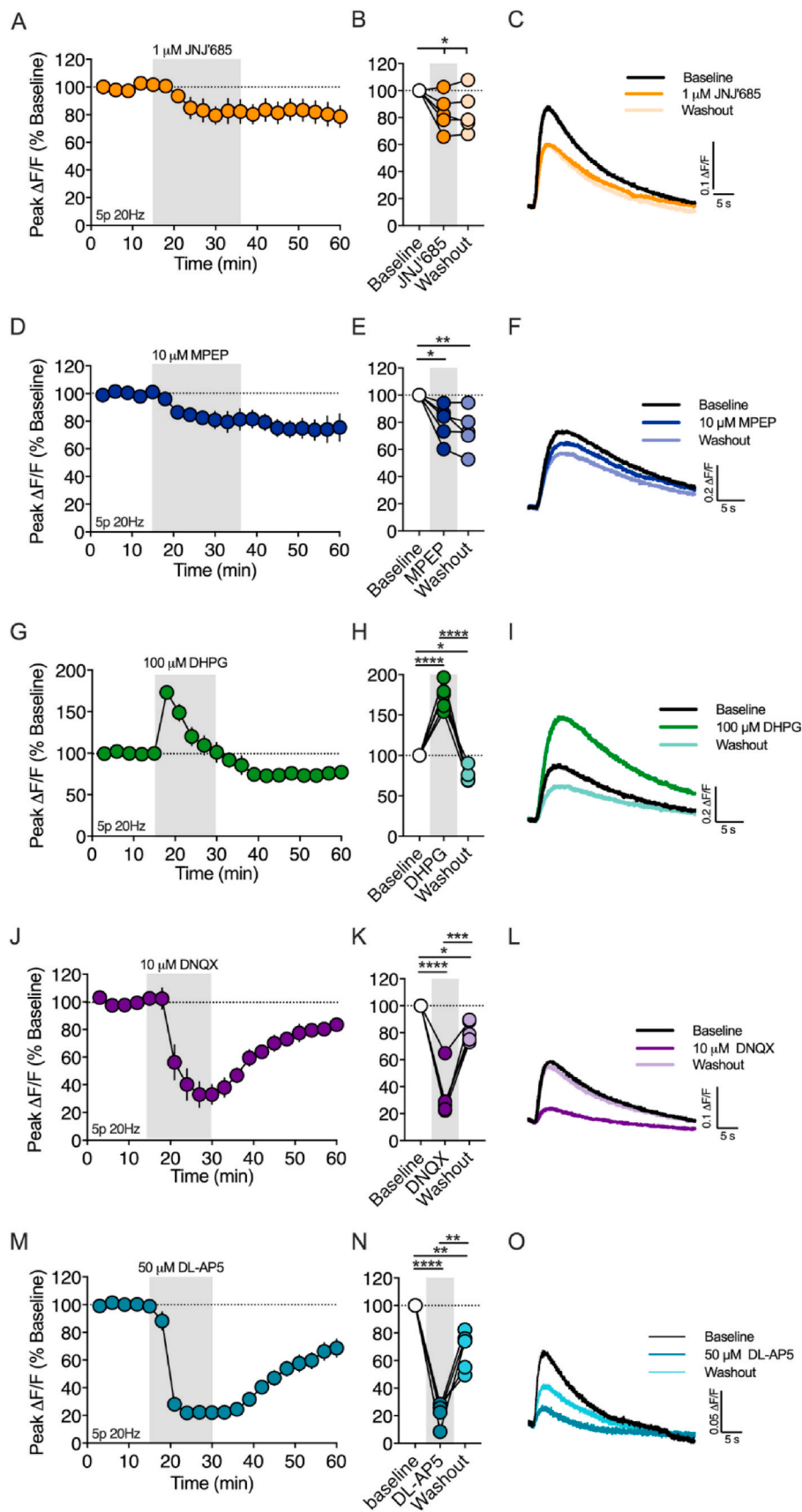
Fig. 4. Synaptically evoked 2-AG transients are dependent on metabotropic and ionotropic glutamate receptors. A) Timecourse of the mGlu1 NAM, JNJ16259685 (JNJ'685), on the amplitude of 2-AG transients evoked by a 5 pulse train at 20Hz (5p 20Hz). Gray shading indicates drug application period. B) Effect of JNJ'685 at the end of the drug application period and a washout period. C) Representative 2-AG transients at baseline and following JNJ'685 bath application or washout. The effect of the mGlu5 NAM, MPEP (D–F), mGlu1/5 agonist, (RS)-DHPG (G–I), AMPA receptor antagonist (J–L) and NMDA receptor antagonist (M–O) were also evaluated. *, $p < 0.05$; **, $p < 0.01$; ***, $p < 0.001$; ****, $p < 0.0001$.

2003). However, few reports directly demonstrate the involvement of AMPARs in eCB production because AMPAR mediated EPSC/EPSP amplitude is a primary measurement for studying eCB physiology at excitatory synapses. With the ability to measure eCB generation directly using GRAB$_{eCB2.0}$, we tested the hypothesis that AMPARs are a primary voltage source for synaptically driven 2-AG production in the DLS (Fig. 4J-L). Bath application of the AMPAR antagonist, DNQX (10 μM), rapidly decreased the amplitude of evoked (5p 20Hz) 2-AG transients to 33.1 ± 8.1% of the baseline amplitude (n = 5 slices, 1-way RM ANOVA, Drug: $F_{(2,8)} = 56.91$, $p < 0.0001$; $p < 0.0001$ compared to baseline), which reversed back towards baseline over a 30 min washout period (81.1 ± 3.4% baseline, $p < 0.0002$ compared to DNXQ). We next tested if AMPAR-dependent depolarization engaged L-type calcium channels (LTCC) leading to 2-AG generation. Bath application of the LTCC blocker, nifedipine (10 μM), did not reduce the amplitude of the evoked 2-AG transient (Supplementry Figs. 1, 94.6 ± 5.5% of baseline, n = 5 slices, 1 sample *t*-test, $t_{(4)} = 0.9772$, $p > 0.05$), suggesting another voltage sensitive calcium channel/receptor may be responsible for triggering 2-AG generation. One possibility is the NMDA receptor (NMDAR). Indeed, bath application of the NMDAR antagonist, DL-AP5 (50 μM), resulted in a rapid reduction in the evoked 2-AG transient to 22.23 ± 8.1% of baseline (Fig. 4M-O, n = 5 slices, 1-way RM ANOVA, Drug: $F_{(2,8)} = 73.02$, $p < 0.0001$; $p < 0.0001$ compared to baseline), which reversed back towards baseline over a 30 min washout period (67.48 ± 7.9% baseline, $p = 0.0003$ compared to DL-APV).

3.3. Muscarinic M1 receptors contribute to synaptically driven 2-AG mobilization

In the dorsal striatum, muscarinic M1 receptors (M1Rs) enhance eCB-dependent DSI (Narushima et al., 2007) and are required for eCB mediated spike timing-dependent plasticity (Fino et al., 2010). On the other hand, M1Rs inhibit HFS-LTD by inhibiting L-type calcium channels (Wang et al., 2006). Given these opposing roles in modulating eCB short-term and long-term plasticity, we investigated the role of M1Rs on 2-AG generation following brief synaptic stimulation (5p 20Hz, Fig. 5). Bath application of the M1R antagonist VU 0255035 (VU′035, 1 μM)

reduced the amplitude of the evoked 2-AG transient to 41.42 ± 7.1% of the baseline (n = 5 slices, 1-way RM ANOVA, Drug: $F_{(2,8)} = 66.37$, $p < 0.0001$; $p = 0.0001$ compared to baseline), which did not washout (Fig. 5A–C, $p = 0.0001$ compared to baseline). To further investigate the role of M1Rs on 2-AG production, we bath applied the M1R positive allosteric modulator (PAM), VU 0486846 (VU′846, 10 μM), which increased the 2-AG peak amplitude to 274.4 ± 40.6% of baseline (Fig. 5D–F, n = 5 slices, 1-way RM ANOVA, Drug: $F_{(2,8)} = 13.36$, $p = 0.003$; $p = 0.003$ compared to baseline). The baseline fluorescence intensity (F) was not changed by VU′035 or VU′846 (data not shown), suggesting that tonic acetylcholine (ACh) release from cholinergic interneurons (CINs) does not generate an eCB tone through M1R stimulation.

3.3.1. M1R and group I mGluRs facilitate 2-AG production by distinct mechanisms

Both M1R and AMPAR antagonists robustly inhibited (>60%) 2-AG production, suggesting these receptors converge on a common signaling mechanism. To investigate this possibility, we measured the effect of the M1R PAM, VU′846, on 2-AG generation while blocking AMPA receptors (Fig. 6A–C). First, DNQX (10 μM) was bath applied, which reduced the 2-AG transient to 38.2 ± 3.0% of baseline (n = 5 slices, 1-way RM ANOVA, Drug: $F_{(2,8)} = 64.54$, $p < 0.0001$; $p < 0.0001$ compared to baseline), a similar magnitude of inhibition as observed in the previous experiment with this antagonist. After the inhibitory effect of DNQX plateaued, VU′846 (10 μM) was co-applied with DNQX. DNQX completely occluded the effect of VU′846 on 2-AG production ($p > 0.05$ compared to DNQX alone), suggesting that M1Rs and AMPARs share a common signaling pathway leading to 2-AG production. It is possible that AMPARs located on CINs are required for driving ACh release rather than directly involved in eCB production in MSNs. To test this hypothesis, we expressed the genetically encoded ACh sensor, GRAB$_{ACh3.0}$ (Jing et al., 2020) in the DLS and measured ACh transients evoked by train stimulation (5 pulses at 20 Hz). Bath application of DNQX (10 μM), did not change the amplitude of the evoked ACh transients (Supplementry Figs. 2, 100.8 ± 2.7% of baseline, n = 3 slices, 1 sample *t*-test, $t_{(2)} = 0.2875$, $p > 0.05$), demonstrating that the role of AMPA receptors in
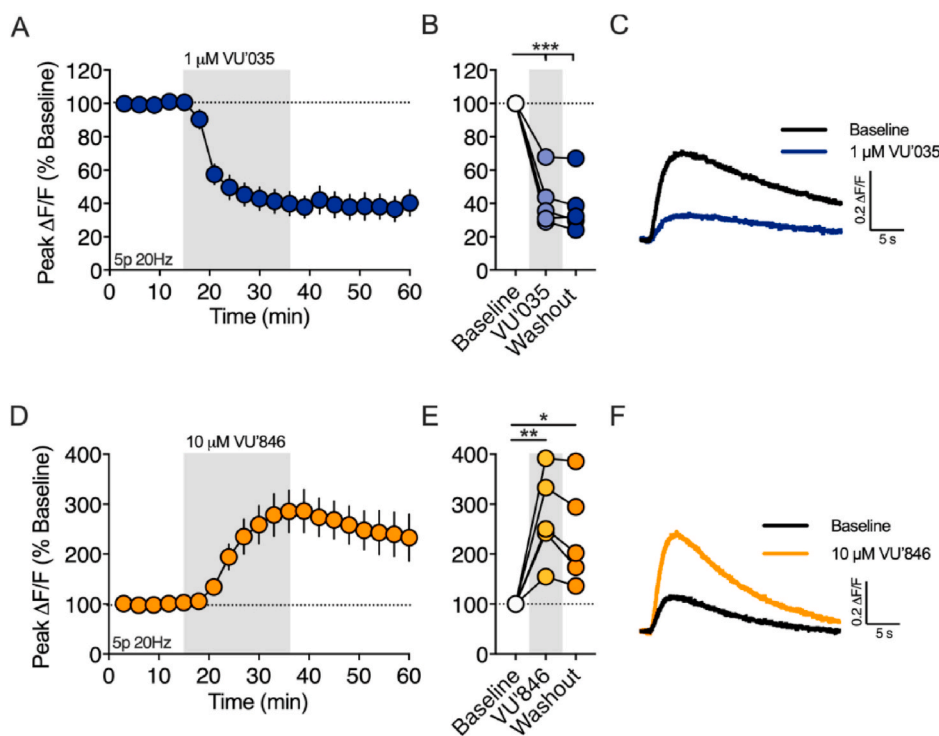

Fig. 5. Muscarinic M1Rs are required for 2-AG generation evoked by brief synaptic stimulation. A) Effect of the M1R antagonist, VU0255035 (VU′035), on the amplitude of 2-AG transients evoked by a 5 pulse train at 20Hz (5p 20Hz). Gray shading indicates drug application period. B) Effect of VU′035 and washout at the end of each drug application period. C) Representative 2-AG transients before and after VU′035 bath application. D-F) Same as above except for the M1R PAM, VU04868486 (VU′846). *, $p < 0.05$; **, $p < 0.01$; ***, $p < 0.001$.
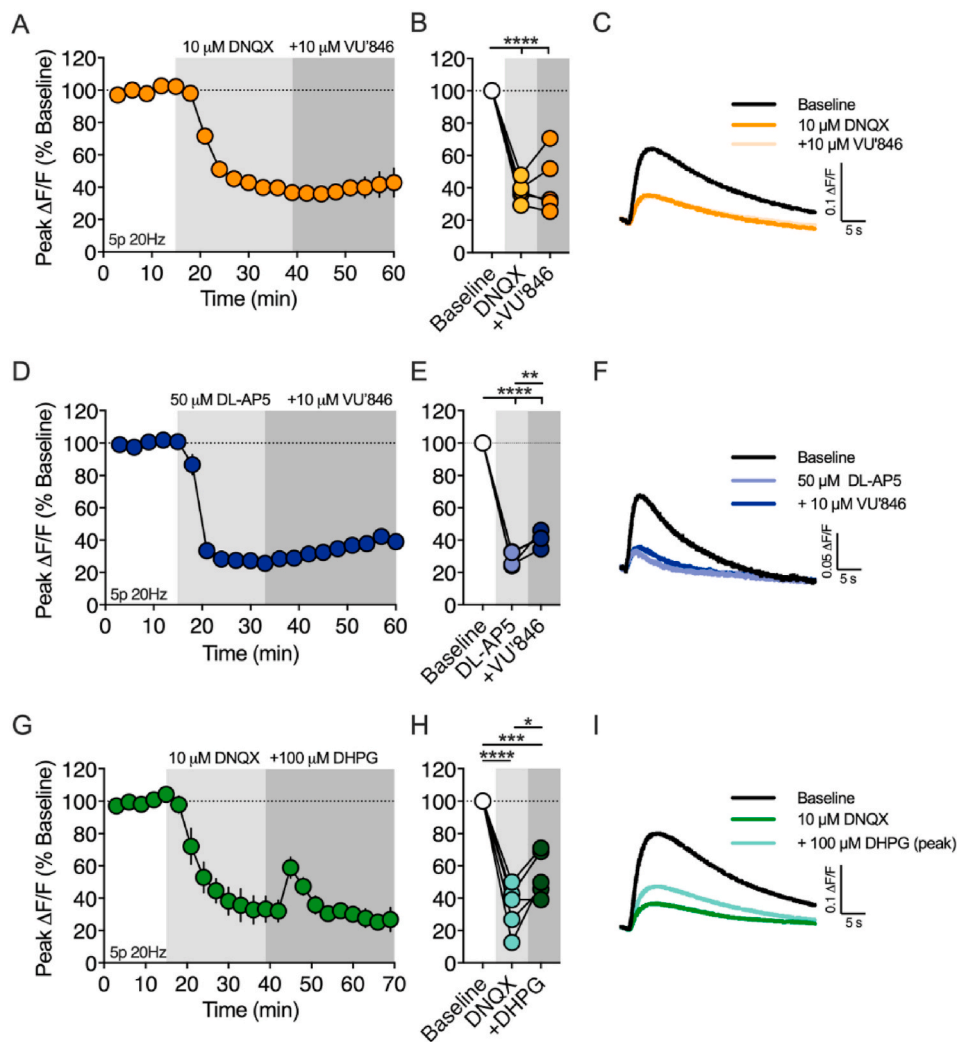
Fig. 6. M1Rs and mGlu1/5s trigger 2-AG mobilization through distinct mechanisms that differentially require ionotropic glutamate receptors. A) Timecourse of the M1R PAM, VU′846, on the amplitude of 2-AG transients in the presence of the AMPAR antagonist, DNQX. 2-AG transients were evoked by a 5 pulse train at 20Hz (5p 20Hz). Gray shading indicates drug application periods. B) Effect of DNQX and DNQX + VU′846 at the end of each drug application period. C) Representative 2-AG transients at baseline, after DNQX and after DNQX + VU′846. D-F) Same as above except VU′846 was bath applied in the presence of the NMDA receptor antagonist, DL-AP5. G-I) Same as A-C except the mGlu1/5 agonist, DHPG, was bath applied in the presence of DNQX. *, $p < 0.05$; **, $p < 0.01$; ***, $p < 0.001$; ****, $p < 0.0001$.

2-AG production is not related to ACh release. Another possibility is that AMPA receptors depolarize the postsynaptic cell allowing NMDA receptor activation and subsequent Ca^{2+} influx that feeds into M1R signaling mechanisms. If this hypothesis is correct, then inhibition of NMDA receptors should also occlude the effect of VU′846 on 2-AG production. Bath application of DL-AP5 (50 μM) reduced the amplitude of the 2-AG transient to $28.6\% \pm 2.3\%$ of baseline (Fig. 6D–F, n = 4 slices, 1-way RM ANOVA, Drug: $F_{(2,6)} = 402.3$, $p < 0.0001$; $p < 0.0001$ compared to baseline), similar to the previous experiment with this antagonist. Subsequent coapplication of VU′846 increased the amplitude of the 2-AG transient to $40.7\% \pm 2.4\%$ ($p = 0.01$ compared to DL-AP5 alone), however this effect was greatly attenuated compared to the previous experiment with VU′846 application alone. Normalizing the 2-AG transient to the amplitude measured at DL-AP5 equilibrium, showed that VU′846 enhanced peak 2-AG production to $144.1 \pm 16.2\%$ compared to $274.4 \pm 40.6\%$ with VU846 application alone.

Given that M1R and mGlu1/5 both couple to $G\alpha_{q/11}$ heterotrimeric g-proteins, we investigated whether (RS)-DHPG enhancement of 2-AG production was also dependent of AMPAR activation. Again, bath application of DNQX (10 μM) reduced the 2-AG transient to $34.2 \pm 6.6\%$ of baseline (n = 5 slices, 1-way RM ANOVA, Drug: $F_{(2,8)} = 56.0$, $p < 0.0001$, $p < 0.0001$ compared to baseline), however co-application of DNQX did not block (RS)-DHPG enhancement of 2-AG production ($p = 0.028$ compared to DNQX, Fig. 6G–I). Normalizing the 2-AG transient to the amplitude measured at DNXQ equilibrium, showed that (RS)-DHPG enhanced peak 2-AG production to $193.9 \pm 51.9\%$ of the DNXQ

baseline, a similar magnitude observed with (RS)-DHPG application alone.

3.4. Dopamine D2 receptors on cholinergic interneurons inhibit 2-AG release

Activation of dopamine D2Rs is required for the expression of HFS-LTD in the dorsal striatum. The mechanism by which D2Rs participate in HFS-LTD has been debated in the literature, however it's clear that D2Rs on cholinergic interneurons are required for inhibiting ACh release and M1R activation (Augustin et al., 2018; Wang et al., 2006). In contrast to HFS-LTD, we found that brief synaptic stimulation requires M1R activation for 2-AG generation. Thus, we hypothesized that D2Rs would inhibit, rather than promote, 2-AG generation following brief synaptic stimulation (5p 20Hz, Fig. 7A–C). Indeed, bath application of the D2R agonist quinpirole (1 μM), reduced the amplitude of evoked 2-AG transients to $61.1 \pm 4.2\%$ of baseline (n = 5 slices, 1-way RM ANOVA, Drug: $F_{(2,8)} = 29.59$, $p = 0.0002$; $p = 0.007$ compared to baseline). The specificity of this action of quinpirole for D2Rs was confirmed by co-application of the D2R antagonist, sulpiride (10 μM), which reversed the effect of quinpirole and subsequently increased the amplitude of the evoke 2-AG transient to $131.4 \pm 11.5\%$ of the initial baseline amplitude ($p < 0.022$ compared to baseline). The rebound effect of sulpiride suggests that 20 Hz electrical stimulation elicits dopamine release from midbrain dopamine (DA) fibers to limit 2-AG generation by acting on D2Rs.
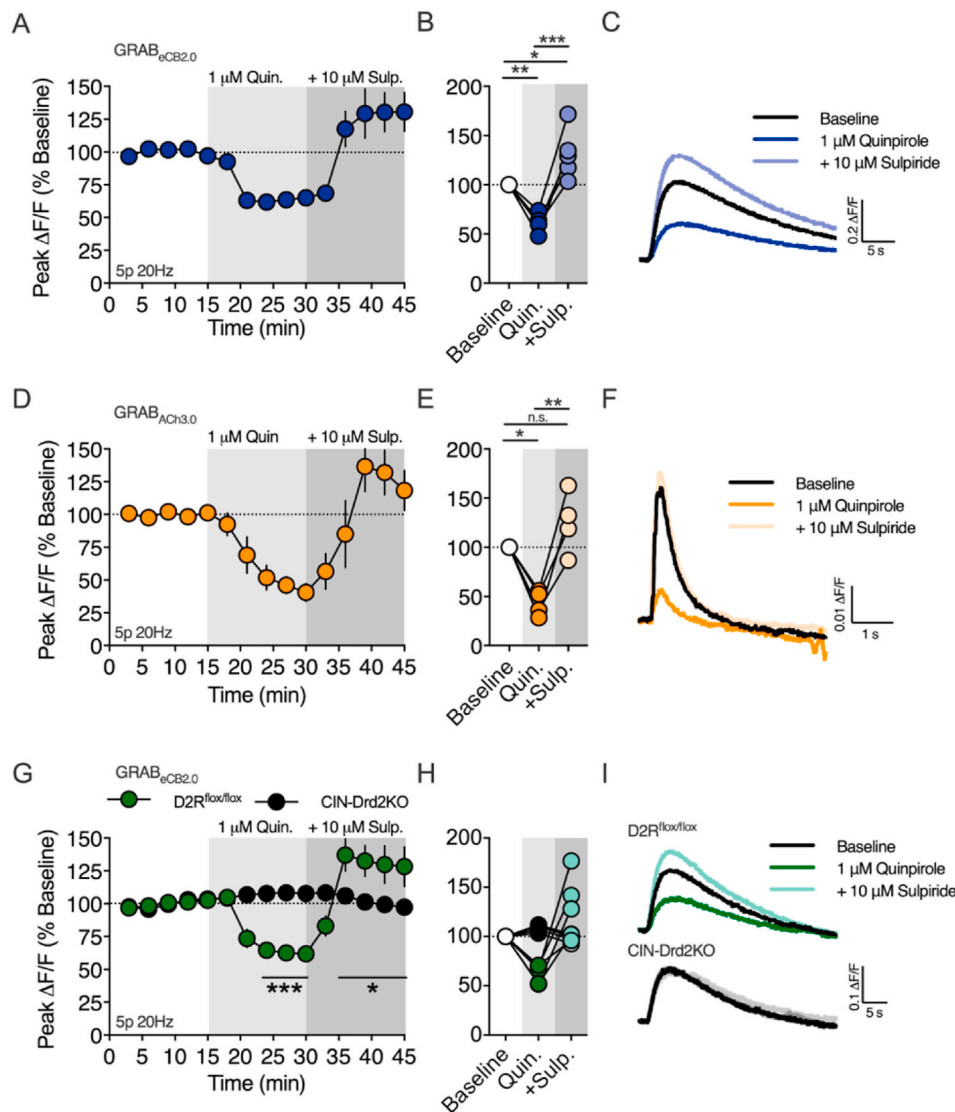
Fig. 7. Dopamine D2 receptors expressed on cholinergic interneurons inhibit 2-AG production. A) Timecourse of the D2R agonist, quinpirole (Quin.), on the amplitude of 2-AG transients evoked by a 5 pulse train at 20Hz (5p 20Hz). The D2R antagonist, sulpiride (Sulp.) was applied after equilibration of the quinpirole effect. Gray shading indicates drug application periods. B) Effect of quinpirole and quinpirole + sulpiride at the end of each drug application period. C) Representative 2-AG transients at baseline, after quinpirole and after quinpirole + sulpiride. D-F) Same as above except the amplitude of acetylcholine (ACh) transients were measured with the genetically-encoded fluorescent sensor, GRAB$_{ACh3.0}$. G-I) Same as in A-C except with slices from D2R$^{flox/flox}$ and CIN-Drd2KO mice. *, $p < 0.05$; **, $p < 0.01$; ***, $p < 0.001$.

Our results showing that M1R inhibition or D2R activation suppresses 2-AG generation is consistent with the hypothesis that D2Rs on CINs are the target of quinpirole and endogenously released DA. To support of this hypothesis, we expressed the ACh sensor, GRAB$_{ACh3.0}$, in the DLS to examine the effect of D2R activation of ACh release (Fig. 7D–F). ACh release evoked by 5 pulse 20 Hz train stimulation was inhibited by bath application of quinpirole (1 μM, 43.3 ± 6.6% of baseline, n = 4 slices, 1-way RM ANOVA, Drug: $F_{(2,6)} = 21.75$, p = 0.0018; p = 0.0102 compared to baseline), which was reversed by the addition of sulpiride (10 μM, 125.2 ± 15.8% of baseline, p > 0.05 compared to baseline).

To further confirm the role of CIN D2Rs on 2-AG production, we bred D2R-flox mice with ChAT-IRES-Cre mice to conditionally knockout D2Rs from CINs (CIN-Drd2KO) and measured the effect of quinpirole and sulpiride on 2-AG production (Fig. 7G–I). Qualitatively, the 2-AG transients evoked in slices from CIN-Drd2KO mice were indistinguishable from 2-AG transients evoked in slices from wildtype C57BL/6J or D2R$^{flox/flox}$ mice. The inhibitory effect of quinpirole (1 μM) on 2-AG production was lost in slices from CIN-Drd2KO mice (n = 4/5 slices/group, 2-way RM ANOVA, Drug: $F_{(14,98)} = 10.23$, p < 0.0001; Genotype: $F_{(1,7)} = 0.7338$, p > 0.05; Interaction: $F_{(14,98)} = 15.14$, p < 0.0001). Additionally, sulpiride (10 μM) did not enhance 2-AG production in slices from CIN-Drd2KO mice. These results confirm that stimulation of

D2Rs on cholinergic interneurons, by either exogenous agonist application or endogenously release DA, inhibit 2-AG generation induced by brief synaptic stimulation.

4. Discussion

In this report, we used the novel fluorescent biosensor, GRAB$_{eCB2.0}$, in combination with brain slice photometry to study eCB signaling dynamics in the DLS. This approach offers several advantages over traditional electrophysiological techniques to studying eCB physiology. For example, we were able to make direct measurements of eCB mobilization at corticostriatal afferents, the primary site of action for eCBs, and were able study eCB mobilization mechanisms without perturbing the postsynaptic neurons. In addition, we examine the roles of ionotropic receptors more thoroughly than in past studies that relied on the function of these receptors as the readout for eCB actions. We show that brief bouts of synaptic stimulation induce long lasting 2-AG transients, which are dependent on convergent signals from ionotropic glutamate receptors and Gα$_{q/11}$ coupled GPCRs. Our data indicate that mGlu1/5 and M1Rs trigger 2-AG mobilization though distinct mechanisms with divergent dependence on AMPAR activation. Furthermore, D2Rs located on CINs inhibit 2-AG transients by limiting ACh release and M1R stimulation. Collectively, this study provides new insights on circuit and

cellular mechanisms controlling 2-AG mobilization in the DLS.

We measured eCB mobilization kinetics following brief, physiologically relevant, synaptic stimulation. Small eCB transients were evoked by paired-pulse stimulation, and increasing the number of stimuli to 5 or 10 pulses produced progressively larger transients that were sensitive to stimulation frequency up to 100 Hz. This dependence on stimulus number and frequency parallels the stimulation dependence of eCB-mediated inhibition of presynaptic Ca^{2+} transients and STD induced by synaptic stimulation in the cerebellum (Brown et al., 2003; Maejima et al., 2001), and spike timing dependent plasticity in striatum, (Cui et al., 2015, 2016), suggesting that the neural activity rules supporting eCB mobilization may be generalized across brain regions. Synaptically-evoked eCB transients were slow compared to the dynamics of many other neurotransmitter systems. The transients took several seconds to reach peak amplitudes and decayed over the course of tens of seconds; kinetics consistent with reported durations of eCB-dependent STD. In contrast, transients evoked by single or multiple stimuli and measured with GPCR-based ACh and DA sensors peak within less than a second and persist for only a few seconds after stimulus cessation (Jing et al., 2020; Patriarchi et al., 2018; Sun et al., 2018). The minimum time from the onset of synaptic stimulation to detecting eCBs at corticostriatal afferents, defined as t_{eCB}, was ~300 ms regardless of stimulation protocol. In our experiments, t_{eCB} represents the cumulative time for glutamate and ACh release, postsynaptic eCB generation, retrograde transit to corticostriatal membranes, and finally activation of $GRAB_{eCB2.0}$. Thus, this measurement likely indicates the minimum time required for eCB-dependent presynaptic inhibition following synaptic stimulation. Consistent with this notion, our measurements of t_{eCB} are similar to estimates of the minimum time required for DSI expression (t_{DSI}) in CA1 pyramidal cells (Heinbockel et al., 2005).

eCB transients evoked by brief synaptic stimulation were sensitive to MAGL inhibition, indicating that 2-AG is mobilized under these conditions. Specifically, when $GRAB_{eCB2.0}$ was expressed in corticostriatal afferents, MAGL inhibition prolonged the decay component of the eCB transient and increased basal fluorescence, consistent with the generation of a 2-AG tone. Furthermore, DAGL inhibition decreased the peak amplitude of the of eCB transient by 75–80%, confirming that 2-AG is the primary eCB evoked by our stimulation protocol. On the other hand, FAAH inhibition, did not significantly affect eCB transients evoked using the same stimulation protocol, suggesting that AEA is not efficiently mobilized.

2-AG transients were dependent on ionotropic and metabotropic glutamate receptors. Inhibition of mGlu5 or mGlu1 decreased the 2-AG transient by 15–20%, while the mGlu1/5 agonist, DHPG, increased the 2-AG transient by 175%. The effect of DHPG was bi-phasic as the initial potentiation of 2-AG generation declined and eventually lead to depression. It is possible that prolonged application of DHPG leads to receptor desensitization effectively reducing mGluR signaling. Supporting this interpretation, the delayed DHPG depression of 2-AG production was similar in magnitude to the inhibition observed with mGluR antagonism. Blocking AMPA receptors decreased the 2-AG transient by 67% indicating that these receptors are indispensable for robust 2-AG generation. A previous study was able to show the involvement of AMPARs in synaptically generated eCB-STD in the cerebellum by optical measurements of presynaptic Ca^{2+} transients, however, AMPARs were only a minor component (Brown et al., 2003). Our experiments suggest that AMPAR activation depolarizes the postsynaptic membrane allowing NMDAR activation and a subsequent rise in intracellular Ca^{2+}, as inhibition of NMDARs decreased the 2-AG transient by 74%.

Muscarinic M1Rs modulate eCB signaling in several brain regions. In the DLS, M1Rs are required for LTD induced by spike timing dependent plasticity protocols (Fino et al., 2010), but suppress LTD induced by HFS (Wang et al., 2006). Furthermore, M1Rs enhance DSI in MSNs and can promote DSE through synergistic actions with mGlu5 (Narushima et al., 2007; Uchigashima et al., 2007). Thus, depending on the eCB induction protocol, M1Rs can either promote or suppress eCB-dependent

plasticity. In the current study, 2-AG transients were robustly inhibited by M1R antagonists and augmented by a M1R PAM, indicating that ACh released from CINs provides a major contribution to 2-AG production induced by brief trains of synaptic stimulation. Our data show that blocking M1Rs, AMPARs or NMDARs inhibited the eCB transient by 60–75%, suggesting these receptors converge on a common signaling pathway leading to eCB production. Indeed, inhibiting AMPARs or NMDARs blocked 2-AG enhancement by the M1R PAM. Our data showing that AMPAR antagonists don't inhibit evoked ACh release, measured with $GRAB_{ACh3.0}$, argue against a role for ionotropic glutamate receptors on CINs in the ACh release that drives M1R activation. Alternatively, activation of AMPARs and NMDARs on MSNs can lead to rises in intracellular Ca^{2+} that may converge with $G\alpha_{q/11}$ signaling mechanisms, leading to 2-AG generation.

Production of 2-AG is thought to involve several Ca^{2+}- and GPCR-dependent mechanisms. These include Ca^{2+} increases independent of GPCRs, Ca^{2+}-independent receptor driven eCB release (Ca^{2+}-independent RER), and Ca^{2+}-assisted receptor-driven eCB release (Ca^{2+}-assisted RER) (Kano, 2014). Previous studies in striatum provide evidence that all three of these mechanisms are in play in striatum. Increased Ca^{2+} induces 2-AG-dependent DSI and DSE in striatum, while the RER and Ca^{2+}-assisted RER mechanisms are implicated in STD and LTD induced by synaptic stimulation and GPCR activation (Hashimotodani et al., 2013; Lerner and Kreitzer, 2012; Narushima et al., 2007; Uchigashima et al., 2007). In the present experiments M1Rs appear to generate 2-AG though a Ca^{2+}-assisted receptor-driven eCB release (Ca^{2+}-assisted RER) mechanism based on the involvement of iGlus. In contrast, the effect of mGlu1/5 stimulation is independent of AMPAR activation as DHPG still enhanced the eCB transient in the presence of AMPAR antagonists, implicating Ca^{2+}-independent RER in the actions of this GPCR. Our findings suggesting that mGlu1/5 signals though a Ca^{2+}-independent RER mechanism is consistent with reports in the hippocampus and cerebellum (Chevaleyre and Castillo, 2003; Kim et al., 2002; Maejima et al., 2001). In the DLS, however, DHPG-induced LTD is dependent on postsynaptic depolarization and L-type calcium channels (Kreitzer and Malenka, 2005). Although these results are in contrast to our observations, in the striatum, mGlu1/5 can trigger eCB-LTD through Ca^{2+}-dependent and Ca^{2+}-independent mechanisms (Lerner and Kreitzer, 2012). The study by Lerner and Kreitzer showed LTD requiring 2-AG mobilization is Ca^{2+} independent, consistent with our findings, while LTD requiring AEA mobilization is Ca^{2+} dependent. Thus, the Ca^{2+} dependence of mGlu1/5 induced eCB mobilization appears to depend on the mechanisms through which postsynaptic cells and receptors are activated, and whether the cellular context favors 2-AG or AEA production.

Activation of D2Rs, by quinpirole application or endogenous DA release, suppressed the amplitude of evoked 2-AG transients. This result was somewhat surprising because D2R activation is required for eCB-dependent LTD in the DLS (Calabresi et al., 1992) and quinpirole inhibits evoked EPSCs in MSNs in a frequency and CB1R-dependent manner (Wang et al., 2012; Yin and Lovinger, 2006). In the context of HFS-LTD, D2Rs expressed on CINs promote eCB signaling by limiting ACh release and subsequent activation of M1Rs located on MSNs (Augustin et al., 2018; Wang et al., 2006), which is opposite to the mechanism uncovered in our study. These independent findings, suggest that M1Rs can either inhibit or augment eCB production, depending on the level of neural activity, and D2Rs regulate the magnitude of eCB modulation by M1Rs regardless of the sign. Importantly, 2-AG is the predominate eCB mobilized following brief synaptic stimulation in our study, while evidence suggests that AEA is the predominate eCB underlying HFS-LTD (Ade and Lovinger, 2007; Lerner and Kreitzer, 2012). Thus, it is conceivable that the D2R-ACh-M1R signaling mechanism differently regulates 2-AG and AEA production. In support of this hypothesis, activation of D2-like DA receptors increases AEA levels in the dorsal striatum and limbic forebrain, while D2R inhibition increases 2-AG content in limbic forebrain (Giuffrida et al., 1999; Patel et al.,

2003). At the molecular level, M1Rs couple to $G\alpha_{q/11}$ so 2-AG production may well occur through the canonical PLC and DAGL pathway. On the other hand, M1Rs can inhibit LTCCs (Howe and Surmeier, 1995; Perez-Burgos et al., 2008), which is the mechanism responsible for suppressing eCB-LTD and presumably AEA production. Interestingly, in our study, 2-AG production required NMDARs, rather than LTCCs, thus different sources of Ca^{2+} influx may contribute to differential regulation of eCBs by M1Rs.

In conclusion, we implemented the novel genetically encoded biosensor, $GRAB_{eCB2.0}$, to uncover unrecognized signaling mechanisms underlying 2-AG production in the DLS. In addition, we made direct measurements of eCB production on physiological time scales, which has not been possible previously. Undoubtedly, $GRAB_{eCB2.0}$ will prove useful in future studies, *in vivo* and in reduced preparations, to gain further insight into eCB signaling under physiological and pathological conditions (Dong et al., 2021).

Author contributions

D.J.L and D.M.L designed the experiments. D.J.L performed the experiments and analyzed the data. A.D. K.H. and Y.L. provided the $GRAB_{eCB2.0}$ and $GRAB_{ACh3.0}$ sensor constructs. H.L.P contributed to sens or validation experiments. D.J.L. and D.M.L wrote the manuscript with input from the other authors.

Declaration of competing interest

Y. L. has filed patent applications, the value of which might be affected by this publication.

Acknowledgements

Appendix A. Supplementary data

Supplementary data to this article can be found online at https://doi.org/10.1016/j.neuropharm.2021.108916.

References

Ade, K.K., Lovinger, D.M., 2007. Anandamide regulates postnatal development of long-term synaptic plasticity in the rat dorsolateral striatum. J. Neurosci. 27, 2403–2409.

Augustin, S.M., Chancey, J.H., Lovinger, D.M., 2018. Dual dopaminergic regulation of corticostriatal plasticity by cholinergic interneurons and indirect pathway medium spiny neurons. Cell Rep. 24, 2883–2893.

Bello, E.P., Mateo, Y., Gelman, D.M., Noain, D., Shin, J.H., Low, M.J., Alvarez, V.A., Lovinger, D.M., Rubinstein, M., 2011. Cocaine supersensitivity and enhanced motivation for reward in mice lacking dopamine D2 autoreceptors. Nat. Neurosci. 14, 1033–1038.

Brown, S.P., Brenowitz, S.D., Regehr, W.G., 2003. Brief presynaptic bursts evoke synapse-specific retrograde inhibition mediated by endogenous cannabinoids. Nat. Neurosci. 6, 1048–1057.

Calabresi, P., Maj, R., Pisani, A., Mercuri, N.B., Bernardi, G., 1992. Long-term synaptic depression in the striatum: physiological and pharmacological characterization. J. Neurosci. 12, 4224–4233.

Calabresi, P., Picconi, B., Tozzi, A., Di Filippo, M., 2007. Dopamine-mediated regulation of corticostriatal synaptic plasticity. Trends Neurosci. 30, 211–219.

Chevaleyre, V., Castillo, P.E., 2003. Heterosynaptic LTD of hippocampal GABAergic synapses: a novel role of endocannabinoids in regulating excitability. Neuron 38, 461–472.

Costa, R.M., Cohen, D., Nicolelis, M.A., 2004. Differential corticostriatal plasticity during fast and slow motor skill learning in mice. Curr. Biol. 14, 1124–1134.

Cui, Y., Paille, V., Xu, H., Genet, S., Delord, B., Fino, E., Berry, H., Venance, L., 2015. Endocannabinoids mediate bidirectional striatal spike-timing-dependent plasticity. J. Physiol. 593, 2833–2849.

Cui, Y., Prokin, I., Xu, H., Delord, B., Genet, S., Venance, L., Berry, H., 2016. Endocannabinoid dynamics gate spike-timing dependent depression and potentiation. Elife 5, e13185.

Dang, M.T., Yokoi, F., Yin, H.H., Lovinger, D.M., Wang, Y., Li, Y., 2006. Disrupted motor learning and long-term synaptic plasticity in mice lacking NMDAR1 in the striatum. Proc. Natl. Acad. Sci. U. S. A. 103, 15254–15259.

Dong, A., He, K., Dudok, B., Farrell, J.S., Guan, W., Liput, D.J., Puhl, H.L., Cai, R., Wang, H., Duan, J., Albarran, E., Ding, J., Lovinger, D.M., Li, B., Soltesz, I., Li, Y., et al., 2021. A fluorescent sensor for spatiotemporally resolved imaging of endocannabinoid dynamics in vitro and in vivo. Nat. Biotechnol. Online ahead of print.

Fino, E., Paille, V., Cui, Y., Morera-Herreras, T., Deniau, J.M., Venance, L., 2010. Distinct coincidence detectors govern the corticostriatal spike timing-dependent plasticity. J. Physiol. 588, 3045–3062.

Galante, M., Diana, M.A., 2004. Group I metabotropic glutamate receptors inhibit GABA release at interneuron-Purkinje cell synapses through endocannabinoid production. J. Neurosci. 24, 4865–4874.

Gerdeman, G.L., Ronesi, J., Lovinger, D.M., 2002. Postsynaptic endocannabinoid release is critical to long-term depression in the striatum. Nat. Neurosci. 5, 446–451.

Giuffrida, A., Parsons, L.H., Kerr, T.M., Rodriguez de Fonseca, F., Navarro, M., Piomelli, D., 1999. Dopamine activation of endogenous cannabinoid signaling in dorsal striatum. Nat. Neurosci. 2, 358–363.

Gubellini, P., Saulle, E., Centonze, D., Bonsi, P., Pisani, A., Bernardi, G., Conquet, F., Calabresi, P., 2001. Selective involvement of mGlu1 receptors in corticostriatal LTD. Neuropharmacology 40, 839–846.

Hashimotodani, Y., Ohno-Shosaku, T., Tanimura, A., Kita, Y., Sano, Y., Shimizu, T., Di Marzo, V., Kano, M., 2013. Acute inhibition of diacylglycerol lipase blocks endocannabinoid-mediated retrograde signalling: evidence for on-demand biosynthesis of 2-arachidonoylglycerol. J. Physiol. 591, 4765–4776.

Heinbockel, T., Brager, D.H., Reich, C.G., Zhao, J., Muralidharan, S., Alger, B.E., Kao, J. P., 2005. Endocannabinoid signaling dynamics probed with optical tools. J. Neurosci. 25, 9449–9459.

Howe, A.R., Surmeier, D.J., 1995. Muscarinic receptors modulate N-, P-, and L-type Ca2 + currents in rat striatal neurons through parallel pathways. J. Neurosci. 15, 458–469.

Jing, M., Li, Y., Zeng, J., Huang, P., Skirzewski, M., Kljakic, O., Peng, W., Qian, T., Tan, K., Zou, J., et al., 2020. An optimized acetylcholine sensor for monitoring in vivo cholinergic activity. Nat. Methods.

Kano, M., 2014. Control of synaptic function by endocannabinoid-mediated retrograde signaling. Proc. Jpn. Acad. Ser. B Phys. Biol. Sci. 90, 235–250.

Kim, J., Isokawa, M., Ledent, C., Alger, B.E., 2002. Activation of muscarinic acetylcholine receptors enhances the release of endogenous cannabinoids in the hippocampus. J. Neurosci. 22, 10182–10191.

Kosillo, P., Zhang, Y.F., Threlfell, S., Cragg, S.J., 2016. Cortical control of striatal dopamine transmission via striatal cholinergic interneurons. Cerebr. Cortex 26, 4160–4169.

Kreitzer, A.C., Malenka, R.C., 2005. Dopamine modulation of state-dependent endocannabinoid release and long-term depression in the striatum. J. Neurosci. 25, 10537–10545.

Kreitzer, A.C., Regehr, W.G., 2001. Retrograde inhibition of presynaptic calcium influx by endogenous cannabinoids at excitatory synapses onto Purkinje cells. Neuron 29, 717–727.

Kupferschmidt, D.A., Lovinger, D.M., 2015. Inhibition of presynaptic calcium transients in cortical inputs to the dorsolateral striatum by metabotropic GABA(B) and mGlu2/3 receptors. J. Physiol. 593, 2295–2310.

Lerner, T.N., Kreitzer, A.C., 2012. RGS4 is required for dopaminergic control of striatal LTD and susceptibility to parkinsonian motor deficits. Neuron 73, 347–359.

Liang, R., Broussard, G.J., Tian, L., 2015. Imaging chemical neurotransmission with genetically encoded fluorescent sensors. ACS Chem. Neurosci. 6, 84–93.

Liput, D.J., 2018. Cre-recombinase dependent germline deletion of a conditional allele in the Rgs9cre mouse line. Front. Neural Circ. 12, 68.

Lovinger, D.M., 2008. Presynaptic modulation by endocannabinoids. Handb. Exp. Pharmacol. 435–477.

Maejima, T., Hashimoto, K., Yoshida, T., Aiba, A., Kano, M., 2001. Presynaptic inhibition caused by retrograde signal from metabotropic glutamate to cannabinoid receptors. Neuron 31, 463–475.

Maejima, T., Oka, S., Hashimotodani, Y., Ohno-Shosaku, T., Aiba, A., Wu, D., Waku, K., Sugiura, T., Kano, M., 2005. Synaptically driven endocannabinoid release requires Ca2+-assisted metabotropic glutamate receptor subtype 1 to phospholipase Cbeta4 signaling cascade in the cerebellum. J. Neurosci. 25, 6826–6835.

Mateo, Y., Johnson, K.A., Covey, D.P., Atwood, B.K., Wang, H.L., Zhang, S., Gildish, I., Cachope, R., Bellocchio, L., Guzman, M., et al., 2017. Endocannabinoid actions on cortical terminals orchestrate local modulation of dopamine release in the nucleus accumbens. Neuron 96, 1112–1126 e1115.

Mathur, B.N., Lovinger, D.M., 2012. Endocannabinoid-dopamine interactions in striatal synaptic plasticity. Front. Pharmacol. 3, 66.

Mizuno, G.O., Unger, E.K., Tian, L., 2019. Real time monitoring of neuromodulators in behaving animals using genetically encoded indicators. In: Compendium of in Vivo Monitoring in Real-Time Molecular Neuroscience, pp. 1–18.

Narushima, M., Uchigashima, M., Fukaya, M., Matsui, M., Manabe, T., Hashimoto, K., Watanabe, M., Kano, M., 2007. Tonic enhancement of endocannabinoid-mediated retrograde suppression of inhibition by cholinergic interneuron activity in the striatum. J. Neurosci. 27, 496–506.

Ohno-Shosaku, T., Maejima, T., Kano, M., 2001. Endogenous cannabinoids mediate retrograde signals from depolarized postsynaptic neurons to presynaptic terminals. Neuron 29, 729–738.

Patel, S., Rademacher, D.J., Hillard, C.J., 2003. Differential regulation of the endocannabinoids anandamide and 2-arachidonylglycerol within the limbic forebrain by dopamine receptor activity. J. Pharmacol. Exp. Therapeut. 306, 880–888.

Patriarchi, T., Cho, J.R., Merten, K., Howe, M.W., Marley, A., Xiong, W.H., Folk, R.W., Broussard, G.J., Liang, R., Jang, M.J., et al., 2018. Ultrafast neuronal imaging of dopamine dynamics with designed genetically encoded sensors. Science 360.

Perez-Burgos, A., Perez-Rosello, T., Salgado, H., Flores-Barrera, E., Prieto, G.A., Figueroa, A., Galarraga, E., Bargas, J., 2008. Muscarinic M(1) modulation of N and L types of calcium channels is mediated by protein kinase C in neostriatal neurons. Neuroscience 155, 1079–1097.

Ravotto, L., Duffet, L., Zhou, X., Weber, B., Patriarchi, T., 2020. A bright and colorful future for G-protein coupled receptor sensors. Front. Cell. Neurosci. 14, 67.

Ronesi, J., Gerdeman, G.L., Lovinger, D.M., 2004. Disruption of endocannabinoid release and striatal long-term depression by postsynaptic blockade of endocannabinoid membrane transport. J. Neurosci. 24, 1673–1679.

Ronesi, J., Lovinger, D.M., 2005. Induction of striatal long-term synaptic depression by moderate frequency activation of cortical afferents in rat. J. Physiol. 562, 245–256.

Sgobio, C., Kupferschmidt, D.A., Cui, G., Sun, L., Li, Z., Cai, H., Lovinger, D.M., 2014. Optogenetic measurement of presynaptic calcium transients using conditional genetically encoded calcium indicator expression in dopaminergic neurons. PLoS One 9, e111749.

Shonesy, B.C., Parrish, W.P., Haddad, H.K., Stephenson, J.R., Baldi, R., Bluett, R.J., Marks, C.R., Centanni, S.W., Folkes, O.M., Spiess, K., et al., 2018. Role of striatal direct pathway 2-arachidonoylglycerol signaling in sociability and repetitive behavior. Biol. Psychiatr. 84, 304–315.

Strobel, B., Miller, F.D., Rist, W., Lamla, T., 2015. Comparative analysis of cesium chloride- and iodixanol-based purification of recombinant adeno-associated viral vectors for preclinical applications. Hum. Gene Ther. Methods 26, 147–157.

Sun, F., Zeng, J., Jing, M., Zhou, J., Feng, J., Owen, S.F., Luo, Y., Li, F., Wang, H., Yamaguchi, T., et al., 2018. A genetically encoded fluorescent sensor enables rapid and specific detection of dopamine in flies, fish, and mice. Cell 174, 481–496 e419.

Sung, K.W., Choi, S., Lovinger, D.M., 2001. Activation of group I mGluRs is necessary for induction of long-term depression at striatal synapses. J. Neurophysiol. 86, 2405–2412.

Uchigashima, M., Narushima, M., Fukaya, M., Katona, I., Kano, M., Watanabe, M., 2007. Subcellular arrangement of molecules for 2-arachidonoyl-glycerol-mediated retrograde signaling and its physiological contribution to synaptic modulation in the striatum. J. Neurosci. 27, 3663–3676.

Ueda, N., Tsuboi, K., Uyama, T., 2013. Metabolism of endocannabinoids and related N-acylethanolamines: canonical and alternative pathways. FEBS J. 280, 1874–1894.

Wang, H., Jing, M., Li, Y., 2018. Lighting up the brain: genetically encoded fluorescent sensors for imaging neurotransmitters and neuromodulators. Curr. Opin. Neurobiol. 50, 171–178.

Wang, W., Dever, D., Lowe, J., Storey, G.P., Bhansali, A., Eck, E.K., Nitulescu, I., Weimer, J., Bamford, N.S., 2012. Regulation of prefrontal excitatory neurotransmission by dopamine in the nucleus accumbens core. J. Physiol. 590, 3743–3769.

Wang, Z., Kai, L., Day, M., Ronesi, J., Yin, H.H., Ding, J., Tkatch, T., Lovinger, D.M., Surmeier, D.J., 2006. Dopaminergic control of corticostriatal long-term synaptic depression in medium spiny neurons is mediated by cholinergic interneurons. Neuron 50, 443–452.

Wilson, R.I., Nicoll, R.A., 2001. Endogenous cannabinoids mediate retrograde signalling at hippocampal synapses. Nature 410, 588–592.

Xiao, X., Li, J., Samulski, R.J., 1998. Production of high-titer recombinant adeno-associated virus vectors in the absence of helper adenovirus. J. Virol. 72, 2224–2232.

Yin, H.H., Davis, M.I., Ronesi, J.A., Lovinger, D.M., 2006. The role of protein synthesis in striatal long-term depression. J. Neurosci. 26, 11811–11820.

Yin, H.H., Lovinger, D.M., 2006. Frequency-specific and D2 receptor-mediated inhibition of glutamate release by retrograde endocannabinoid signaling. Proc. Natl. Acad. Sci. U. S. A. 103, 8251–8256.